Variable-range hopping conduction in epitaxial CrN(001)

X. Y. Zhang, J. S. Chawla, B. M. Howe, and D. Gall

Phys. Rev. B **83**, 165205 — Published 25 April 2011

DOI: 10.1103/PhysRevB.83.165205

Variable-range hopping conduction in epitaxial CrN(001)

X.Y. Zhang,[1] J.S. Chawla,[1] B.M. Howe,[2] D. Gall[1]
[1]Department of Materials Science and Engineering,
Rensselaer Polytechnic Institute, Troy, NY 12180, USA
[2]Department of Materials Science and the Frederick Seitz Materials Research Laboratory,
University of Illinois, 104 South Goodwin Avenue, Urbana, Illinois 61801, USA

Abstract

Epitaxial CrN(001) layers, grown by dc magnetron sputtering on MgO(001) substrates at growth temperatures T_s = 550-850 °C, exhibit electronic transport that is dominated by variable-range-hopping (VRH) at temperatures <120 K. A transition from Efros-Shklovskii (ES) to Mott VRH at 30±10 K is well described by a universal scaling relation. The localization length decreases from 1.3 nm at T_s = 550 °C to 0.9 nm for T_s = 600-750 °C but increases again to 1.9 nm for T_s = 800-850 °C, which is attributed to changes in the density of localized states associated with N-vacancies that form due to kinetic barriers for incorporation and enhanced desorption at low and high T_s, respectively. The low-temperature transport data provides lower limits for the CrN effective electron mass of $4.9m_e$, the donor ionization energy of 24 meV, and the critical vacancy concentration for the metal-insulator transition of 8.4×10^{19} cm^{-3}. The room temperature conductivity is dominated by Hubbard band states near the mobility edge and decreases monotonically from 137 Ω^{-1}cm^{-1} for T_s = 550 °C to 14 Ω^{-1}cm^{-1} for T_s = 850 °C, due to a decreasing structural disorder, consistent with the measured x-ray coherence length that increases from 7 to 36 nm for T_s = 550 to 850 °C, respectively, and a carrier density that decreases from 4×10^{20} to 0.9×10^{20} cm^{-3}, as estimated from optical reflection and Hall effect measurements. The absence of an expected discontinuity in the conductivity at ~280 K suggests that epitaxial constraints suppress the phase transition to a low-temperature orthorhombic antiferromagnetic phase, such that CrN remains a cubic paramagnetic insulator over the entire measured temperature range of 10-295 K. These results contradict previous experimental studies that report metallic low-temperature conduction for CrN, but support recent computational results suggesting a band gap due to strong electron correlation and a stress induced phase transition. *PACS*: 72.80.Ga; 72.20.Ee; 61.72.jd

I. Introduction

Chromium nitride (CrN) attracts increasing interest as a potential electronic or spintronic material, due to its magnetic ordering and possible bandgap which make it a promising material for dilute magnetic semiconductors, particularly when combined with (or doped into) other nitride semiconductors.[1-3] However, several discrepancies have emerged regarding the electronic properties of CrN, whose reported values for room temperature resistivity ρ range over five orders of magnitudes, from 3×10^{-4} to 20 Ωcm,[1,4-16] with the most reliable data for single crystal CrN layers in the narrower range of 1.7×10^{-3} to 3.5×10^{-1} Ωcm.[1,9-11,15,16] The temperature dependence of ρ is another controversial point, showing metallic behavior with $d\rho/dT > 0$ in some studies,[10,11,13] but an increase in ρ with decreasing temperature in other reports,[1,4,9,16] which has been attributed to the presence of a band gap[9] or carrier localization due to grain boundaries[14] or N-vacancies.[12] In addition, most $\rho(T)$-curves show a discontinuity at 260-280 K,[1,10-12] which is associated with a magnetic and structural phase transition with a Néel temperature T_N = 273-286 K, from a paramagnetic NaCl structure at room temperature to a low-temperature antiferromagnetic orthorhombic P_{nma} phase[13, 17 - 19] with a 0.56%-0.59% increase of atomic density,[13,19] and a 25% lower bulk modulus.[20] Electronic structure calculations indicate that a distorted antiferromagnetic $[110]_2$ phase is energetically more stable than paramagnetic, ferromagnetic, antiferromagnetic $[110]_1$, or disordered magnetic CrN,[21-23] and magnetic stress relief couples magnetic ordering with the structural change during the phase transition,[24] which may also be induced by increasing the pressure above ~1 GPa.[20] Photoemission data[25] on polycrystalline CrN suggests a metallic antiferromagnetic phase below T_N and a correlated (charge transfer) insulator with a Coulomb energy of 4.5 eV above T_N, in agreement with calculations using a Hubbard Coulomb interaction term U = 3-5 eV,[22] which results in the depletion of electron states near the Fermi-level and the opening of a gap, which is consistent with our recent optical study showing vibrational modes and direct interband transitions that suggest an indirect room temperature bandgap for CrN of 0.19±0.46 eV,[26] however, with an uncertainty that is larger than the gap value, such that the question regarding a bandgap or a band overlap is not resolved with certainty.

In this article, we present the results of an investigation where epitaxial CrN(001) is used to study the electron transport properties from 10 K to room temperature. The epitaxial system with MgO(001) substrates is purposely chosen, because it suppresses the structural phase transition. Thus, the room-temperature cubic phase remains stable over the entire investigated temperature range, facilitating low temperature transport measurements of the cubic NaCl-structure CrN phase. Low temperature transport is attributed to localized N-vacancy defect states that facilitate variable range hopping (VRH) with a crossover at 30±10 K from Efros-Shklovskii (ES) to Mott VRH. The nitrogen vacancy concentration increases both at high and low growth temperatures, $T_s > 800$ °C and $T_s < 600$ °C, due to N_2 desorption and kinetically limited N_2 dissociation, respectively, which causes a sharp increase in the localization length ξ and a correspondingly higher hopping conduction. In contrast, the room temperature conductivity is dominated by electrons that are thermally activated from localized states in the band tail to extended states above the mobility edge. The density of defect states in the conduction band tail decreases with increasing growth temperature, causing a decrease in the room temperature carrier density, which is estimated from Hall effect and optical reflectance measurements to be on the order of 10^{20} cm^{-3}, resulting in an increase in the resistivity by an order of magnitude, from 7.3 to 71 mΩcm. These results demonstrate how strongly the defect density affects CrN transport properties, and explains the large discrepancy in the previously reported room temperature values.

II. Experimental procedure

CrN layers, 0.14 and 1.0 μm thick, were grown in a load-locked ultra high vacuum dc magnetron sputtering system,[27] with a base pressure of 1.3×10^{-7} Pa (1×10^{-9} Torr), onto one-side polished $10\times10\times0.5$ mm^3 MgO(001) wafers that were cleaned, mounted, and degassed for epitaxial growth as described in Ref. 28. Deposition was performed at substrate temperatures T_s in the range of 550-850 °C, in 0.39 Pa (3 mTorr) 99.999% pure N_2 that was further purified through a Micro Torr purifier. A 5-cm-diameter 99.95% pure Cr target was positioned 10.5 cm from the substrate at an angle of 45°, and a constant magnetron power of 350 W was applied, yielding a growth rate of 22 nm/min, as determined from thickness measurements by Rutherford backscattering spectroscopy (RBS). These deposition conditions are expected to yield stoichiomtetric CrN with a N:Cr ratio of 1.00 ± 0.06, based on our previous studies,[9,15] and consistent with RBS results from calibration samples. The surface roughness of the 140-nm-thick CrN layers is <3 nm, based on our previous *in situ* scanning tunneling microscopy and atomic force microscopy studies on samples grown under comparable conditions.[29,30]

The crystalline quality of the layers was investigated by x-ray diffraction (XRD) ω-2θ and ω rocking curve scans in a PANanalytical X'Pert Pro diffractometer with a Cu $K\alpha$ source equipped with an x-ray mirror, an asymmetric two-bounce monochromator ($\lambda_{K\alpha1}$ = 1.5406 Å) with a 0.0068° divergence, a point detector with a 0.04° soller slit, and a custom built cold stage. The XRD measurements were performed using 1.0 μm thick CrN layers. This larger thickness (in comparison to the 140-nm-thick samples used for electric transport measurements) provides sufficient intensity of the CrN 002 peak, so that it can be clearly separated and quantified from the MgO 002 substrate peak.

DC conductivity measurements were performed in a Cryomagnetics Inc ^{4}He cryostat system, which provided a variable temperature at the sample surface ranging from 10 K to room temperature. For these electric measurements, samples were cut into 1 cm long and 0.3 cm wide stripes. Four Cu contacts were sputter deposited onto the CrN in a linear four-point probe geometry. The samples were then mounted onto a sample holder using silver paint to maximize thermal contact, and electric contacts were completed using four copper wires and silver paint. The conductivity was measured continuously during warming up from 10 K, using a Keithley 2400 source meter which operated as both a voltmeter and a current source with I = 0.1-1 μA. Hall effect measurements at 300 K were performed on two samples with growth temperatures of 600 and 800 °C in a Quantum Design physical property measurement system. Contacts were deposited in a Van der Pauw geometry and the Hall resistance determined from a linear fit of the measured Hall voltage as a function of the magnetic field which was continuously varied from -7 to 7 T as described in Ref. 31.

Optical reflectance was measured with a Nicolet Magna IR-560 Fourier Transform Infrared (FTIR) spectrometer over the wavelength range λ = 12-25 μm, corresponding to wavenumbers of 400-833 cm^{-1}, using an incident angle of 45°.

III. Results

Figure 1(a) is a portion of a typical XRD ω-2θ scan, obtained from a 1.0-μm-thick CrN/MgO(001) layer grown at T_s = 850 °C and plotted on a log scale. The only peaks that are detected in the measured 2θ range from 20 to 80° are the MgO 002 and CrN 002 reflections, at

$2\theta = 42.90°$ and 43.26°, respectively. This corresponds to a measured MgO lattice constant of 0.4211 nm, close to the literature value of 0.4212 nm[32] or 0.4213 nm,[33] and an out-of-plane CrN lattice constant of 0.4179 nm. This is in the range of reported bulk values, 0.4133–0.4185 nm,[10,15,34-36] but likely indicates a slight compressive strain due to differential thermal contraction during cooling from the 850 °C growth temperature, similar to what has been previously reported for epitaxial CrN grown on MgO(001).[15] We note here that no secondary impurity phase is detected by XRD for all layers in this study. This is in disagreement with results in Ref. 15, which show considerable nitrogen loss and possible impurity phases for $T_s > 700$ °C. The most likely cause for this disagreement is a difference in the absolute temperature calibration for these different experiments, but other parameters like deposition rate and plasma density which determine ion flux and energy as well as atomic nitrogen flux may affect the driving force for nitrogen loss in the deposited layer.

The inset in Fig. 1(a) is a ω-rocking curve of the CrN 002 reflection at a constant $2\theta = 43.26°$, showing a peak with a full width at half maximum (FWHM) of $\Gamma_\omega = 0.33°$. This value is considerably larger than the width due to the beam divergence of the diffractometer, the acceptance angle of the detector, and the mosaicity of the MgO substrate, which exhibits a measured rocking curve width <0.1° for all samples (not shown). Thus, the measured value for Γ_ω provides direct information on the crystalline quality of the layers. It is plotted in Figure 1(b) for four 1.0-μm-thick CrN layers grown at different temperatures T_s but otherwise identical conditions. It decreases approximately linearly with T_s, from 1.74 to 0.97 to 0.74 to 0.33° for T_s = 550, 650, 750, and 850 °C, respectively. The right y-axis indicates the corresponding in-plane XRD coherence length $\eta_{\|} = \lambda/(2\Gamma_\omega \sin\omega)$,[37] which increases from $\eta_{\|}$ = 7 to 12, 16, and 36 nm. We attribute the lower crystalline quality at lower T_s to the presence of 1D and 2D crystalline defects, which are dislocations and low-angle grain boundaries, respectively. The defect density decreases with increasing T_s, due to the increasing adatom diffusion length which yields larger atomically smooth growth fronts, as well as due to the larger dislocation mobility at higher temperature which facilitates low-angle grain boundary migration.

In order to confirm the absence of a possible structural phase transition around 280 K, XRD ω-2θ scans were performed at a reduced temperature of 253 K (not shown). The measured out-of-plane lattice parameter was 0.04% smaller than the measured room-temperature value, which is attributed to the thermal contraction upon cooling. A phase transition to the reported low-temperature orthorhombic structure is expected to cause a 60× larger change (i.e. a reduction of 2.4%) in the lattice parameter, indicating that the samples in our study show no structural phase transition.

Fig. 2(a) is a plot of the measured low temperature conductivity σ_{10K} at 10 K, and room temperature conductivity σ_{290K} at 290 K, as a function of the growth temperature. σ_{10K} decreases from 0.17 Ω^{-1}cm^{-1} at T_s = 550 °C to a minimum of 0.021 Ω^{-1}cm^{-1} at T_s = 700 °C and increases again to 0.19 Ω^{-1}cm^{-1} at T_s = 850 °C. This is attributed to localized states associated with point defects and short range disorder, as discussed in detail below. σ_{290K} decreases monotonically from 137 Ω^{-1}cm^{-1} for T_s = 550 °C to 14 Ω^{-1}cm^{-1} for T_s = 850 °C. Thus, changing the growth temperature causes the room temperature conductivity to vary by an order of magnitude, suggesting that transport in CrN strongly depends on crystalline quality and/or N-vacancy concentration. Based on this result, it is not surprising that previous reports on the room temperature conductivity for epitaxial CrN(001) vary widely, with values of 13,[9,15] 56,[10] and 588 Ω^{-1}cm^{-1}.[11] Our current values fall within the range of these reports.

Corresponding room temperature Hall effect measurements on samples grown at $T_s = 600$ and 800 °C (not shown) indicate that the Hall mobility μ_H is very small, with values of 0.16±0.11 and 0.19±0.40 cm^2/Vs, respectively. The trend as a function of T_s cannot be determined from these measurements, because the measured μ_H is of comparable magnitude as the experimental uncertainty. Thus, the Hall measurements primarily provide an upper bound for μ_H on the order of 0.1 cm^2/Vs. Such a small mobility is typical for conduction dominated by localized states, as observed for example for amorphous germanium.[38] It is consistent with the T-dependent transport measurements and is attributed to thermally activated electrons near the mobility edge, as discussed in the next section.

Figure 2(b) is a semi-log plot of the measured conductivity σ vs $1/T$, for 140 nm thick CrN layers grown at different $T_s = 550$-850 °C. The plotted open symbols are a subsection of the measured conductivity values, while the lines are obtained by fitting to the data for $T < 120$K, as described below. All samples show a monotonous increase in σ with increasing T over the complete measured temperature range $T = 10$-295 K, and exhibit no discontinuity near 280 K that could be attributed to a magneto-structural phase transition. This is in contrast to some previously reported studies[1,10-14,25] and confirms the absence of a phase transition in our epitaxial layers, as discussed in more detail in the discussion section. The absolute values as well as the T-dependence of σ are affected by the growth temperature. For example, the conductivity at 290 K is by a factor of 800, 3200, and 70 larger than that at 10 K, for $T_s = 550$, 700, and 850 °C, respectively. The plotted slopes continuously increase with T for all samples, indicating that the temperature dependence of the conductivity cannot be explained by thermal activation across a single band gap. Correspondingly, the exponent γ in

$$\sigma = \sigma_\infty \times \exp[-(T_o/T)^\gamma] \qquad (1)$$

is smaller than unity for all samples. Here, σ_∞ and T_o are normalization constants for conductivity and temperature, respectively, and $\gamma = 1$, ½, or ¼ for thermally activated charge carrier generation and variable range hopping (VRH) with and without significant electron-electron interactions, respectively.

In particular, Mott VRH predicts a $\gamma = 1/4$ such that[39-41]

$$\sigma = \sigma_M \times \exp[-(T_M/T)^{1/4}], \qquad (2)$$

while Efros-Shklovskii (ES) hopping includes a coulomb gap due to electron-electron interactions such that[42,43]

$$\sigma = \sigma_{ES} \times \exp[-(T_{ES}/T)^{1/2}]. \qquad (3)$$

Here σ_M, T_M, σ_{ES}, T_{ES} are conductivity and temperature normalization constants for Mott and ES VRH, respectively. In order to explore if the low temperature transport mechanism in CrN can be described by VRH, we plot log(σ) vs $T^{-1/4}$ and vs $T^{-1/2}$, as shown Figs. 3(a) and 3(b), respectively, for three exemplary samples with T_s = 550, 700, and 850 °C. The straight lines through the data in Fig. 3(a) indicate that Eq. (2) describes the temperature dependence well for 50 K < T < 120 K, but overestimates σ at low T, and deviates from the measured data for approximately T > 120 K. In contrast, the data for T < 25 K is well described with a straight line in Fig. 3(b). These results indicate that the CrN electronic transport is dominated by ES VRH for T < 25 K, by Mott VRH for 50 K < T < 120 K, and by an additional conduction mechanism at high temperature, as discussed in the discussion section. Table I lists values for T_M and T_{ES}, obtained using linear fitting within these temperature ranges as shown in Fig. 3. Both T_M and T_{ES} increase with increasing T_s = 550-700 °C, but decrease for T_s = 700-850 °C. This general trend, with a maximum at T_s = 700 °C, is attributed to changes in the nitrogen vacancy density, as discussed in the following section. The Mott temperature T_M is proportional to the fraction of space that is occupied by wavefunctions at the Fermi-level, that is, the cube of the localization length ξ divided by the density of states at the Fermi level $N(E_F)$ according to[40]

$$kT_M \approx 18/N(E_F)\xi^3 \ . \tag{4}$$

It also provides information on the Mott hopping distance $R_{h,M}$ and hopping energy $W_{h,M}$ according to[40]

$$R_{h,M} \approx 0.4\xi(T_M/T)^{1/4} \text{ and} \tag{5}$$

$$W_{h,M} \approx 0.24kT^{3/4}T_M^{1/4} \ . \tag{6}$$

The values for the ratio $R_{h,M}/\xi$ from Eq. (5) depend on T_s and range from 1.5-2.6 at 120 K and increase to 2.0-3.4 at 40 K. That is, all samples exhibit a hopping distance that is larger than the localization length within the temperature range for which we consider Mott VRH to be dominant, satisfying the criterion for VRH.[44] At low temperature, electron-electron interactions become important as the hopping energy becomes smaller than the Coulomb gap Δ_{CG} given by[45]

$$\Delta_{CG} \approx k\left(T_{ES}^3/T_M\right)^{\frac{1}{2}} \ . \tag{7}$$

That is, at T below a transition temperature T^* so that $W_{h,M} < \Delta_{\mathrm{CG}}$, electron interactions are significant and the electron transport is described by ES VRH. Table I lists the values for $T^* \approx 16T_{ES}^2/T_M$, which are consistent with the approximate transition temperature of 30±10 K, obtained from the analysis in Fig. 3.

Fig. 4 is a plot of the localization length ξ vs T_s, showing the highest value of 1.9 nm at T_s = 850 °C and a minimum of ξ = 0.87 nm for the sample grown at 700 °C. The right y-axis indicates a corresponding lower limit estimate for the nitrogen vacancy concentration, as discussed in the next section. ξ is obtained using[43]

$$kT_{ES} \approx 2.8e^2/\varepsilon\xi, \tag{8}$$

where $\varepsilon = \varepsilon_h + 4\pi\chi$ is the static low temperature CrN dielectric constant, ε_h the host static dielectric constant, and $\chi = e^2N(E_F)\xi^2$ the contribution due to electrons in the localized states.[46] We use $\varepsilon_h = 53$, based on the room-temperature optical analysis of a 11 μm thick CrN layer with a free carrier density $<3\times10^{19}$ cm^{-3} (Ref. 26) and assuming that ε_h is temperature independent between 0 and 300 K, which has been shown to be valid to within 4% for various semiconductors.[47] Combining Eqs. (4) and (8) yields values for ξ, as plotted in Fig. 4 and listed in Table I, as well as values for $N(E_F)$, which exhibit no clear trend with T_s and have a typical value of $6\pm2\times10^{45}$/Jm^3. In addition, we obtain values for ε ranging between 72 and 132. That is, ε is only 1.4-2.5× larger than ε_h, indicating that all of our CrN samples are far from the critical region for a metal-insulator transition, as discussed in the next section.

We use a universal scaling relation to describe the crossover from the low-temperature ES to the higher-temperature Mott VRH, following the example of similar transitions that have previously been reported for doped semiconductor materials.[45,48,] The following expression was first proposed by Aharony *et al.*:[49]

$$\ln(\sigma_o/\sigma) = Af(T/T_x). \tag{9}$$

σ_o, A and T_x are material-dependent scaling factors and $f(x)$ is a universal function, given by[49]

$$f(x) = \frac{1+[(1+x)^{1/2}-1]/x}{[(1+x)^{1/2}-1]^{1/2}}. \tag{10}$$

The measured conductivity data is fitted using equations (9) and (10) for each sample individually over the temperature range 10-120 K. The resulting curves are plotted as solid lines in Fig. 2(b), while the fitting parameters σ_o, A and T_x are presented in Table II. In order to illustrate how well the data is described by this formalism, Fig. 5 shows a log-log plot of the normalized conductivity vs the normalized temperature. The data for all samples collapse on the universal curve which corresponds to $f(x)$. The fitting also provides values for the Mott and ES characteristic temperatures,[49] obtained using $T'_M = A^4 T_x$ and $T'_{ES} = 9A^2 T_x / 2$ and listed in Table II. The values for T'_{ES} are comparable to those for T_{ES} in Table I, except for $T_s \geq 800$ °C. This discrepancy at high T_s is associated with the very small values for T_x, which suggest that the crossover temperature is well below the lowest experimental $T = 10$ K, using an estimate for the crossover temperature of 4-200×T_x according to Ref. 49. In contrast, T'_M is much smaller than T_M, which is consistent to previous reports on CdSe[49] and ZnO[50] and may be due to neglecting higher temperature thermal excitations.[49]

Figure 6 is a plot of the optical reflectance in the infrared wavelength range $\lambda = 12$-25 µm, from 140-nm-thick CrN/MgO(001) layers grown at $T_s = 550$-850 °C. All spectra exhibit a local maximum around $\lambda = 13$ µm and a reflectance edge at $\lambda = 14$-18 µm. The feature at 13 µm is associated with a drop in the refractive index[26] and the resulting interference effects between the reflection from the layer surface and the layer/substrate interface, while the increase to a high reflection above 18 µm is primarily attributed to lattice vibrations. In particular, the spectra for $T_s = 800$ and 850 °C show a maximum around $\lambda = 23.5$ µm, consistent with a transverse optical phonon mode at the zone center at a frequency of 11.7 THz.[26] In contrast, R for $T_s = 550$-750 °C monotonously increases even for $\lambda = > 18$ µm, which we attribute to an additional contribution from free carriers. The increase above the strong reflection plateau is most evident for the $T_s = 550$ °C sample and occurs at $\lambda > 19$ µm, while the onset increases to $\lambda = 21$ µm for $T_s = 600$ and 650 °C, and $\lambda = 23$ µm for $T_s = 700$ and 750 °C. This suggests that the room temperature free carrier density N_e decreases with increasing T_s, which is consistent with the room temperature transport measurements, as discussed in more detail below. At wavelengths where the free carrier contribution is negligible, like for example at $\lambda = 18$ µm, R increases with increasing T_s.

We attribute this to the increasing crystalline quality that results in a stronger dielectric response associated with the lattice vibrations.

IV. Discussion

In this section, we discuss first the VRH that dominates low temperature conductivity, secondly the mechanism for room temperature transport, and lastly how our results compare with previous reports on insulating and metallic CrN in the paramagnetic and antiferromagnetic phases. The T-dependence of the conductivity of our CrN layers indicates variable range hopping for $T < 120$ K, with a transition from ES to Mott VRH around 30 K, as illustrated in Fig. 3. This crossover temperature for VRH is considerably higher than that reported for doped semiconductors such as n-GaAs,[51] Si:B,[48] Si:As,[52] n-CdSe,[45] Ge:As[53] and Si:P,[54] but is comparable to that of oxides including $Sr_2Y_{0.5}Ca_{0.5}Co_2O_7$,[55] In_xO_y[56] and ZnO.[50] The relatively high crossover temperature indicates strong electron-electron interactions which we attribute to the relatively flat d-bands in CrN. VRH is commonly observed for both doped and non-crystalline semiconductors when point-defects and dopants cause localized states in the band gap, and the density of states is finite (i.e. does not vanish) at the Fermi level.[39,40] We attribute the localized states in crystalline CrN to native defects, particularly nitrogen vacancies which are common in NaCl-structure transition metal nitrides like TiN,[57] ScN[58] or TaN.[59] They act as donors[12] and may cause carrier localization.[22,59] The localization length ξ increases with increasing donor (i.e. N-vacancy) concentration N_v according to[60,61]

$$\xi(N_v) = \xi_o(1-N_v/N_c)^{-\upsilon}, \tag{11}$$

where the scaling exponent υ is predicted theoretically to be unity,[62] while experimental studies on doped semiconductors report $\upsilon = 0.5\text{-}1$.[60, 63-65] With this scaling behavior, ξ diverges as N_v

approaches a critical concentration N_c for the metal-insulator transition, but reaches a constant ξ_o, which is equal to the effective Bohr radius a_B,[60] for small N_v, as the overlap between localized electron states becomes negligible. The plot in Fig. 4 shows that T_s = 700 and 850 °C lead to the smallest and largest localization lengths of 0.87 and 1.9 nm, respectively, corresponding to the smallest and largest N-vacancy concentrations. In order to estimate N_c, we note that $4\pi\chi$ tends to infinity as N_v approaches N_c, and that $4\pi\chi$ = 19 and 79 for the 700 and 850 °C samples, respectively. Thus, the 700 °C sample is farther away from N_c so that a_B is smaller than, but likely close to, 0.87 nm. The distance between nitrogen vacancies d is smaller than the variable-range-hopping distance $R_{h,M}$ for all T_s, since all samples exhibit VRH. Thus, d is smaller than the smallest $R_{h,M}$, which we calculate using Eq. (5) for T_s = 700 °C and T = 120 K to be 2.3 nm. Therefore, the critical distance between nitrogen vacancies $d_c < d <$ 2.3 nm. The Mott criteria[39] $N_c^{1/3}a_B = 0.25$, suggests that $d_c = 4a_B$, assuming a simple-cubic arrangement of vacancies, which yields $a_B <$ 0.57 nm, consistent with the upper bound for a_B of 0.87 nm, derived above. Correspondingly, the lower limit for $N_c = 8.4\times10^{19}$ cm^{-3}. We also obtain, using the simple hydrogen model,[66] lower limits for the effective electron mass in CrN of $4.9m_e$, and the donor ionization energy of 24 meV. However, the hydrogen model may not be well suited to estimate the effective mass and donor/acceptor ionization energy, since a_B is not much larger than the lattice constant of 0.414 nm.[67] We determine the lower bound for N_v for each sample with Eq. (11), assuming $\upsilon = 1$ and setting $\xi_o = a_B <$ 0.57 nm and correspondingly $N_c > 8.4\times10^{19}$ cm^{-3}. This yields lower bounds for N_v is in the range of 3-6×10^{19} cm^{-3}, as indicated with the right y-axis in Fig. 4, showing the lowest and highest N-vacancy concentrations for T_s = 700 and 850 °C, respectively.

At low temperature, where VRH dominates electron transport, a higher nitrogen vacancy concentration leads to a higher CrN conductivity, as evident when comparing Figs. 2(a) and 4, where both $\sigma_{10\text{K}}$ and N_v curves exhibit a U-shape with conductivity and vacancy concentration being nearly constant between T_s = 600-700 °C with $\sigma_{10\text{K}} = 0.028\pm0.006\ \Omega^{-1}\text{cm}^{-1}$ and $N_v = 3.1\pm0.2\times10^{19}\ \text{cm}^{-3}$, respectively, and the minimum for both curves being at T_s = 700 °C. We attribute the steep increase in N_v at $T_s \approx 800$ °C to a reduced nitrogen incorporation during growth, associated with temperature activated N-N association and successive N_2 desorption at the growing CrN(001) surface, consistent with previous reports indicating a loss of nitrogen in CrN_x with increasing T_s.[13] Similarly, we attribute the high $\sigma_{10\text{K}}$ and N_v values at T_s = 550 °C to N vacancies that are the result of a limited N-incorporation during low temperature growth, where N_2 dissociation at the growing CrN surface is kinetically limited. Overall, $\sigma_{10\text{K}}$ and ξ (or N_v) agree well, with the exception of the sample grown at 800 °C, which we attribute to T = 10 K being too high to truly represent low temperature: The low slope of the T_s = 800 °C curve at 10 K in Fig. 2(b), and the low T_{ES} value in Table I for T_s = 800 °C, indicate that decreasing T below 10 K would yield a relatively high conductivity in comparison to the T_s < 800 °C samples, consistent with the result in Fig. 4.

In the following, we discuss the dominant conduction mechanism at room temperature. VRH does not explain the T-dependence of σ for T > 120 K, since the exponent γ from Eq. (1) is larger than ½, as evident in Fig. 3. Previous studies[10,22] on CrN have attributed the temperature dependence of the conductivity to thermally activated carriers across a conventional band gap E_g and determined values of E_g = 20-40 meV[9,22] and 71 meV.[10] If using a comparable analysis, i.e. setting the slope at room temperature in Fig. 2(b) equal to $-E_g/2k$, we obtain E_g values that are consistent with these previously published values and range from 48 to 81 meV, with the smallest and largest values for the samples grown at T_s = 850 and 700 °C, respectively. However, we do not believe that a thermally activated interband transition dominates room temperature conduction in CrN, since this should lead to a conductivity that only weakly depends on defect concentration, in clear contradiction to the measured $\sigma_{290\mathrm{K}}$ varying by an order of magnitude in our samples, as shown in Fig. 2(a). In addition, the measured Hall mobility $\mu_H \approx 0.1$ cm^2/Vs is well below reported values of 11, 5.8 and 86 cm^2/Vs for related NaCl-structure transition metal nitrides, ScN,[68] TiN,[68] and HfN,[31] respectively, suggesting that the charge carriers in our CrN layers do not occupy completely delocalized states as is the case for these related nitrides with conventional conduction bands. Therefore, we explore in the following three conduction processes that include carrier localization. They have been reported for doped semiconductors[39] and become increasingly important with increasing temperature, including (i) nearest neighbor hopping (NNH), where electrons jump from one localized state near the Fermi level to a neighboring defect site, (ii) thermal activation of electrons from the Fermi level to the mobility edge in the upper Hubbard band,[41] and (iii) donor ionization. We first reject process (i) as a viable explanation for the room temperature transport in CrN. If NNH is the dominant transport mechanism, then the sample with the highest N-vacancy concentration should exhibit the highest conductivity. Based on the data in Fig. 4 and the discussion above, T_s = 850 °C yields the highest vacancy concentration, however, it has the lowest room temperature conductivity as shown in Fig. 2(a). That is, our data is inconsistent with conduction by NNH.

In contrast, process (ii) can reasonably explain room temperature conduction in our samples: As described by Mott[41] for doped crystalline semiconductors,[69] the perturbation in the electron potential due to structural disorder causes Anderson localization[70] in the not fully occupied lower Hubbard band. However, if the bandwidths B_1 and B_2 of the upper and lower

Hubbard bands are sufficiently broad, that is when $(B_1 + B_2)/2$ approaches the Hubbard energy U,[39-41] the two Hubbard bands overlap, yielding delocalized states in the mid-band region (that is, also in the upper Hubbard band), resulting in a mobility edge which separates localized and delocalized states. Thermal activation of carriers from the Fermi level E_F to this mobility edge at an energy E_C results in conduction, however, with a Hall mobility that is typically rather small, with reported values in the order of 0.1 cm^2/Vs.[39,71] Our Hall measurements, with 300 K values of $\mu_H = 0.16 \pm 0.11$ and 0.19 ± 0.40 cm^2/Vs for $T_s = 600$ and 800 °C, respectively, indicate also a Hall mobility of the order of 0.1 cm^2/Vs, suggesting that thermal activation to the mobility edge in a localized system may be responsible for the room temperature conduction in our CrN layers. The activation energy, obtained from the slope of $\ln\sigma$ vs $1/kT$ at room temperature, varies between 24.0 and 40.6 meV for the seven samples grown at $T_s = 550\text{-}850$ °C.

The third process (iii), which is the donor ionization conduction process where electrons are thermally excited from the Fermi level to the conduction band, cannot be excluded with complete certainty as the dominant room temperature CrN conduction process. In that case, the activation energy $E_A = 24.0\text{-}40.6$ meV corresponds to the donor ionization energy. The above estimation for E_A using low-temperature transport data provides a lower bound of 24 meV, which would be consistent with the measured E_A values. However, as discussed above, transport in a conventional band as is the case for process (iii) is expected to yield a carrier mobility that is 1-3 orders of magnitude higher than the measured $\mu_H = 0.1$ cm^2/Vs. Thus, we conclude that process (ii) is most likely the dominant room temperature transport process in our CrN samples.

The free carrier density N_e at room temperature can be estimated from both, our optical and our Hall effect measurements. We assume that the increase in reflectance on top of the resonance due to lattice polarization at large wavelengths in Fig. 6 is a contribution from free carriers, and obtain N_e from the plasma frequency $\omega_p = (N_e e^2/\varepsilon_0\varepsilon_r m^*)^{1/2}$, using an estimated $\varepsilon_r = 30$ (Ref. 26) for screening by valence electrons and using the lower bound for the effective mass $m^* = 4.9m_e$ from above. This yields an estimated N_e that decreases from 4.5×10^{20} cm^{-3} for T_s = 550 °C to 3.7×10^{20} cm^{-3} for T_s = 600-650 °C, 3.1×10^{20} cm^{-3} for T_s = 700-750 °C, and possibly 2.8×10^{20} cm^{-3} for T_s = 800-850 °C. The last value is rather uncertain because it is unclear if the slight increase in R at λ = 24 μm for the T_s = 800 and 850 °C spectra is just due to experimental noise. In order to estimate N_e from the Hall coefficient R_H, we note that for localized systems $R_\text{H} \neq 1/eN_e$ and even the carrier type cannot be determined from the sign of R_H. However, it is known that $\mu_\text{H}/\mu \approx 1/10$ for electrons at the mobility edge,[39,71] where μ is the conductivity mobility. Thus, we calculate $\mu = 10\mu_\text{H}$ = 1.6 and 1.9 cm^2/Vs for T_s = 600 and 800 °C, respectively, and obtain $N_e = 4\times10^{20}$ and 0.9×10^{20} cm^{-3} from $\sigma_{290\text{K}}$ = 92 and 28 $\Omega^{-1}\text{cm}^{-1}$, respectively. These values for N_e agree rather well with the optical data, both in the order of magnitude ($N_e \approx 10^{20}$ cm^{-3}) as well as in the fact that N_e decreases with increasing T_s. We note that the largest value for $N_e = 4.5\times10^{20}$ cm^{-3} is 4× larger than the estimated lower bound for N_c, while the sample still exhibits insulator behavior. This suggests that N_c may be considerably higher than our lower bound estimate and/or Anderson localization causes insulating behavior despite $N_e > N_c$.[72] We also note that the lower bound for the N-vacancy concentration N_v in Fig. 4 is 2-10 times smaller than N_e, and that the monotonous decrease in the room temperature carrier density N_e vs T_s is not matched by the U-shape of the N_v vs T_s curve, obtained from the low-temperature transport analysis. These facts indicate, that room temperature transport is more strongly affected by crystalline defects like dislocations and small angle grain boundaries, as suggested by the comparable trends for crystalline quality in Fig. 1(b) and $\sigma_{290\text{K}}$ in Fig. 2(b), than by the N-vacancy density.

Finally, we discuss our data in comparison with previously reported transport properties of CrN layers, focusing particularly on aspects where different studies obtained different results including (1) the large variation in room temperature resistivity, (2) the presence or absence of a phase transition, (3) the large variation in the low temperature resistivity, and (4) the conclusion whether CrN is metallic or insulating.

(1) Room temperature resistivity: There exists a wide range of reported room temperature resistivity values for single crystal CrN layers, ranging over 2.5 orders of magnitude from 1.7×10^{-3} to 3.5×10^{-1} Ωcm,[1,9-11,15,16] This large range suggests that this is a controversial matter. However, the resistivity values in this study alone vary by an order of magnitude by simply changing the deposition temperature, from 7.3×10^{-3} Ωcm for T_s = 550 °C to 7.1×10^{-2} Ωcm for T_s = 850 °C. Thus, the room temperature resistivity of CrN depends strongly on the crystalline quality which increases with T_s for our samples. The large range of reported values is therefore not surprising, considering that CrN has been synthesized with very different techniques. In contrast, the reported slope of $\ln\rho$ vs $1/kT$ at room temperature, which is a measure of the apparent activation energy for conduction varies over a much narrower range, with reported values of 20 meV,[9, 22] 35 meV,[10,25] 45 meV,[4] and 75 meV. [73] The values from the present study, 24.0 to 40.6 meV, are fully consistent with these reported values. As discussed above, we attribute the activation energy to a transition from the Fermi level to the mobility edge in the upper Hubbard band.

(2) Phase transition. Various studies on the T-dependent electron transport of CrN report a discontinuity in the ρ vs T curves around the Néel temperature of 280 K, associated with the phase transition from a paramagnetic cubic NaCl structure at high temperature to a distorted orthorhombic antiferromagnetic phase at low temperature. The antiferromagnetic phase has been

found to have a resistivity that is by 10%,[1] 20%,[11,25] 30%,[13] or 120%,[10] lower than the paramagnetic phase. In contrast, our epitaxial CrN layers exhibit no phase transition, as determined by XRD experiments, and also show no discontinuity in the resistivity that could be associated with such a phase transition. This is in agreement with a few reports[9,11,16] that also observe no discontinuity in the ρ vs T curves. We attribute the absence of a phase transition to epitaxial constraints that suppress the shear deformation into the orthorhombic structure. The reasons why some CrN samples show a phase transition while others do not is not fully clear, but may be explained as follows: Most polycrystalline CrN should exhibit the phase transition since individual grains distort in different directions and the associated volume reduction would provide sufficient space within the microstructure for grain boundary slide. In contrast, we envision that a perfect CrN single crystal that is “attached” to a substrate will not distort into the orthorhombic phase, because two of its three crystal axes are fixed by the substrate. However, if voids exist within the single crystal or if easy dislocation motion facilitates slip along {110} planes, then orthorhombic domains may develop within the CrN such that the phase transition occurs, as has been reported for some epitaxial CrN layers.

(3) Low-temperature resistivity: The reported low temperature resistivity values for CrN vary widely and a direct comparison is limited because of the different investigated minimum temperatures. Reported values range from 0.008, 0.013 and 0.02 Ωcm at 77 and 20 and 4 K from Refs. 10, 1, and 25 respectively, to 1.0 and 270 Ωcm at 50 and 20 K from Refs. 16 and 9, respectively, with a particularly high value of 44 kΩcm at 20 K for polycrystalline CrN from Ref. 4. The former low resistivity values (0.008-0.02 Ωcm) are for samples which show a transition to the antiferromagnetic phase, while the latter higher values (1.0-270 Ωcm) are for the cubic CrN phase. Our 10 K resistivity values range from 5.8 to 45 Ωcm, which is consistent with the latter

reported values. That is, our data supports the literature which indicates that samples that remain in their cubic phase exhibit a 2-5 orders of magnitude higher low-temperature resistivity than those that are antiferromagnetic at low temperature. Also, our results suggest that low temperature transport in CrN is dominated by hopping conduction and is therefore strongly affected by the N-vacancy concentration which, in turn, is strongly affected by deposition conditions such as temperature. It is therefore no surprise that reported low temperature resistivity values for CrN vary widely.

(4) Metallic or insulating CrN: The question whether intrinsic CrN is metallic or insulating is still controversial, which we attribute to (1) some samples exhibiting a phase transition while others remain in their paramagnetic cubic structure below the Néel temperature and (2) transport properties being strongly affected by the CrN synthesis method because (2a) the hopping conduction is controlled by the N-vacancy concentration which may be below or above the critical value for a metal-insulator transition and (2b) the tendency for CrN to exhibit Anderson localization due to crystalline defects that form during synthesis. In particular, studies on samples that show a phase transition report $d\rho/dT < 0$ (Refs. 1,25,73) or $d\rho/dT > 0$ (Refs. 10,11,13) for the antiferromagntic low temperature phase. However, according to Ref. 25, the fact that $d\rho/dT < 0$ can be attributed to the presence of disorder, and the antiferromagnetic phase should be considered metallic because $d(\ln\sigma)/d(\ln T) \rightarrow 0$ as $T \rightarrow 0$.[74] Thus, based on this more rigorous definition of a metal, we believe that all reported antiferromagnetic CrN can be considered metallic. In contrast, our results on cubic paramagnetic CrN is insulating, even using the more rigorous definition for an insulator. This result is consistent with other reports of CrN which remain cubic at low temperature.[9,16] It is also consistent with various reports that show $d\rho/dT < 0$ (Refs. 1,9,10,12,14,73) above the Néel temperature, where CrN is in the paramagnetic

phase. However, these latter reports alone could not conclude that paramagnetic CrN is insulating, because the transport data is limited to temperatures above the Néel temperature. In addition, there are some studies that find $d\rho/dT > 0$ above the Néel temperature.[11,13] We believe that this is likely due to (i) a N-vacancy concentration that is above the critical concentration for the Mott metal-insulator transition which we estimate to be on the order of 10^{20} cm^{-3}, and/or (ii) the disorder is sufficiently high to cause delocalization, that is an Anderson metal insulator transition.[72] In summary, based on previously reported transport data as well as the results in the present study, the antiferromagnetic CrN phase is metallic while the paramagnetic phase is insulating. However, the metallic antiferromagnetic phase may exhibit a $d\rho/dT < 0$, due to Anderson localization associated with a sufficiently high crystalline imperfection. Conversely, the insulating paramagnetic phase may also show $d\rho/dT > 0$, if the N-vacancy concentration is above the critical value for the metal insulator transition.

V. Conclusion

XRD and electron transport measurements indicate that single-crystal CrN(001) layers grown on MgO(001) by reactive sputtering at T_s = 550-850 °C exhibit no phase transition at the previously reported Néel temperature around 280 K. This is attributed to epitaxial constraints causing these layers to remain in their cubic paramagnetic phase over the investigated temperature range between 10 K and room temperature. Electron transport below ~120 K is described by variable range hopping with Mott and ES VRH dominating above and below a crossover temperature of 30±10 K. The crossover is well described by a universal scaling and fitting the two regimes with $\ln\sigma \propto -(1/T)^{1/4}$ and $\ln\sigma \propto -(1/T)^{1/2}$ provides values for the localization length ξ which varies from 0.87 to 1.9 nm depending on T_s. The hopping conduction is attributed to nitrogen vacancies. A lower bound for the critical vacancy concentration for the metal-insulator transition is estimated to be 8.4×10^{19} cm^{-3}, and the upper limit for the Bohr radius is 0.57 nm. The estimated lower bound for the nitrogen vacancy concentration N_v depends on T_s and is in the range of 3-6×10^{19} cm^{-3}.

The room temperature conductivity decreases monotonically from 137 $\Omega^{-1}cm^{-1}$ for T_s = 550 °C to 14 $\Omega^{-1}cm^{-1}$ for T_s = 850 °C. This is attributed to the increasing crystalline quality, as quantified by XRD ω-rocking curve scans. Crystalline defects, in particular low-angle grain boundaries cause localized and delocalized states in the band tail which dominate room temperature electron transport through thermal activation from the Fermi level to the mobility edge which divides extended and localized states in the upper Hubbard band. This is supported by the low value of the measured Hall mobility of 0.1 cm^2/Vs. The room temperature carrier density ranges from 0.9-4.5×10^{20} cm^{-3}, as estimated from both Hall measurements and optical reflectance in the infrared.

The overall results show that electron transport in CrN is strongly affected by both the N-vacancy concentration as well as the density of crystalline defects. This explains why previous reports show large differences in both the absolute values as well as in the T-dependence of the resistivity. The data also strongly suggests that cubic paramagnetic CrN exhibits a bandgap, in agreement with recent electronic structure calculations[22] and optical analyses.[26]

Acknowledgements

This research was supported by the National Science Foundation, under grant No. 0645312. We appreciate the help from S. Kar and K.M. Lewis for the temperature dependent transport measurements. B.M.H. gratefully acknowledges the support of the U.S. Department of Defense Science, Mathematics, and Research for Transformation (SMART) scholarship program.

References

[1] P.A. Anderson, R.J. Kinsey, S.M. Durbin, M. Markwitz, J. Kennedy, A. Asadov, W. Gao and R.J. Reeves, J. Appl. Phys. **98,** 043903 (2005).

[2] A. Ney, R. Rajaram, S.S.P. Parkin, T. Kammermeier, and S. Dhar, Appl. Phys. Let. **89**, 112504 (2006).

[3] A. Ney, R. Rajaram, S.S.P. Parkin, T. Kammermeier, and S. Dhar, Phys. Rev. B **76**, 035205 (2007).

[4] P. S. Herle, M. S. Hegde, N. Y. Vasathacharya, S. Philip, M. V. R. Rao, and T. Sripathi, J. Solid State Chem. **134**, 120 (1997)

[5] P. Panjan, B. Navisek, A. Cvelbar, A. Zalar, and J. Vlcek, Surf. Coat. Technol. **98**, 1497 (1998).

[6] K. K. Shih, D. B. Dove, and J. R. Crowe, J. Vac. Sci. Technol. A **4**, 564 (1986).

[7] M. Cekada, P. Panjan, B. Navinsek, and F. Cvelbar, Vacuum **52**, 461 (1999).

[8] R. Mientus and K. Ellmer, Surf. Coat. Technol. **116-119**, 1093 (1999).

[9] D. Gall, C.-S. Shin, R. T. Haasch, I. Petrov, and J. E. Greene, J. Appl. Phys. **91**, 5882 (2002).

[10] C. Constantin, M. B. Haider, D. Ingram, and A. R. Smith, Appl. Phys. Lett. **85**, 6371 (2004).

[11] K. Inumaru, K. Koyama, N. Imo-oka, and S. Yamanaka, Phys. Rev. B **75**, 054416 (2007).

[12] C. X. Quintela, F. Rivadulla, and J. Rivas, Appl. Phys. Lett. **94**, 152103 (2009).

[13] J. D. Browne, P. R. Liddell, R. Street, and T. Mills, Phys. Status Solidi **1**, 715 (1970).

[14] Y. Tsuchiya, K. Kosuge, Y. Ikeda, T. Shigematsu, S. Yamaguchi, and N. Nakayama, Mater. Trans., JIM **37**, 121 (1996).

[15] D. Gall, C.-S. Shin, T. Spila, M. Odén, M.J.H. Senna, J.E. Greene, and I. Petrov, J. Appl. Phys. **91**, 3589 (2002).

[16] R. Sanjinés, O. Banakh, C. Rojas, P. E. Schmid, and F. Lévy, Thin Solid Films **420-421**, 312 (2002).

[17] L. M. Corliss, N. Elliott, and J.M. Hastings, Phys. Rev. **117**, 929 (1960).

[18] R. M. Ibberson and R. Cywinski, Physica B **181**, 329 (1991).

[19] M. N. Eddine, F. Sayetat, and E. F. Bertaut, C. R. Seances Acad. Sci., Ser. B **269**, 574 (1969).

[20] F. Rivadulla, M. Banobre-Lopez, C. X. Quintela, A. Pineiro, V. Pardo, D. Baldomir, M. A. Lopez-Quintela, J. Rivas, C. A. Ramos, H. Salva, J.S. Zhou and J. B. Goodenough, Nature Materials, **8**, 947 (2009).

[21] A. Filippetti, W. E. Pickett, and B. M. Klein, Phys. Rev. B **59**, 7043 (1999).

[22] A. Herwadkar and W. R. L. Lambrecht, Phys. Rev. B **79**, 035125 (2009).

[23] B. Alling, T. Marten, and I. A. Abrikosov, Phys. Rev. B **82**, 184430 (2010).

[24] A. Filippetti and N. A. Hill, Phys. Rev. Lett. **85**, 5166 (2000).

[25] P. A. Bhobe, A. Chainani, M. Taguchi, T. Takeuchi, R. Eguchi, M. Matsunami, K. Ishizaka, Y. Takata, M. Oura, Y. Senba, H. Ohashi, Y. Nishino, M. Yabashi, K. Tamasaku, T. Ishikawa, K. Takenaka, H. Takagi, and S. Shin , Phys. Rev. Lett. **104**, 236404 (2010).

[26] X.Y. Zhang and D. Gall, Phys. Rev. B **82**, 045116 (2010).

[27] C.P. Mulligan, T.A. Blanchet, and D. Gall, Surf. Coat. Technol. **203,** 584 (2008).

[28] J.M. Purswani, T. Spila, and D. Gall, Thin Solid Films, **515**, 1166 (2006).

[29] X.Y. Zhang and D. Gall, Thin Solid Films, **518**, 3813 (2010).

[30] J.R. Frederick, J. D'Arcy-Gall, and D. Gall, Thin Solid Films, **494**, 330 (2006).

[31] H.-S. Seo, T.-Y. Lee, J. G. Wen, I. Petrov, J. E. Greene, and D. Gall, J. Appl. Phys. **96**, 878 (2004).

[32] O. Madelung, U. Rössler, and M. Schulz, Semiconductors: II-VI and I-VII Compounds, Landolt-Börnstein - Group III Condensed Matter, Volume 41B, Springer-Verlag (1999).

[33] The value for a_{MgO}=4.213 Å is from the Inorganic Index to Powder Diffraction (Joint Committee on Powder Diffraction Standards, International Center for Powder Diffraction Data, Newtown Square, PA, 1998): MgO (Card No. 04-0829).

[34] P. Hones, M. Diserens, R. Sanjines, and F. Levy, J. Vac. Sci. Technol. B **18**, 2851 (2000).

[35] P. M. Fabis, R. A. Cooke, and S. McDonough, J. Vac. Sci. Technol. A **8**, 3819 (1990).

[36] The value for a_{CrN} = 4.14 Å is from the Inorganic Index to Powder Diffraction (Joint Committee on Powder Diffraction Standards, International Center for Powder Diffraction Data, Newtown Square, PA, 1998): CrN (Card No. 11-0065, 76-2494).

[37] D. Gall, I. Petrov, N. Hellgren, L. Hultman, J.-E. Sundgren, and J. E. Greene, J. Appl. Phys. **84**, 6034 (1998).

[38] A. H. Clark, Phys. Rev. **154**, 750 (1967).

[39] N. F. Mott and E. A. Davis, "Electronic Processes in Non-Crystalline Materials", 2nd ed., Clarendon, Oxford, (1979).

[40] N. F. Mott, "Metal-Insulator Transitions", 2nd ed. Taylor & Francis, Bristol, PA, USA (1990).

[41] N. F. Mott, "Conduction in Non-Crystalline Materials", 2nd ed., Clarendon, Oxford, UK (1993).

[42] A. L. Efros and B. I. Shklovskii, J. Phys. C **8**, L49 (1975).

[43] B. I. Shklovskii and A. L. Efros, "Electronic Properties of Doped Semiconductor", Springer-Verlag, Berlin, (1984).

[44] C. J. Adkins, in Hopping and Related Phenomena, edited by H. Fritzsche and M. Pollak, World Scientific, Singapore (1990).

[45] Y. Zhang, P. Dai, M. Levy and M. P. Sarachik, Phys. Rev. Lett. **64**, 2687 (1990).

[46] T. G. Castner, in "Hopping Transport in Solids", edited by M. Pollak and B. I. Shklovskii, North-Holland, Amsterdam (1991).

[47] G. A. Samara, Phys. Rev. B **27**, 3494 (1983).

[48] J. G. Massey and M. Lee, Phys. Rev. Lett. **75**, 4266 (1995).

[49] A. Aharony, Y. Zhang, and M. P. Sarachik, Phys. Rev. Lett. **68**, 3900 (1992).

[50] Y. -L. Huang, S. -P. Chiu, Z. -X. Zhu, Z. -Q. Li, and J. -J. Lin, J. Appl. Phys. **107**, 063715 (2010).

[51] B. Capoen, G. Biskupski, and A. Briggs, Solid State Commun. **113**, 135 (2000).

[52] I. Shlimak, M. Kaveh, R. Ussyshkin, V. Ginodman, S. D. Baranovskii, P. Thomas, H. Vaupel, and R. W. van der Heijden, Phys. Rev. Lett. **75**, 4764 (1995).

[53] I. Shlimak, M. Kaveh, M. Yosefin, M. Lea, and P. Fozooni, Phys. Rev. Lett. **68**, 3076 (1992).

[54] M. Hering, M. Scheffler, M. Dressel1, and H. V. Löhneysen, Phys. Rev. B **75**, 205203 (2007).

[55] K. Yamaura, D.P. Young, and R.J. Cava, Phys. Rev. B **63**, 64401 (2001).

[56] R. Rosenbaum, Phys. Rev. B **44**, 3599 (1991).

[57] C.-S. Shin, S. Rudenja. D. Gall, N. Hellgren, T.-Y. Lee, I. Petrov, and J. E. Greene, J. Appl. Phys. **95**, 356 (2004).

[58] A. R. Smith, H.A.H. Al-Brithen, D.C. Ingram, and D. Gall, J. Appl. Phys. **90**, 1809 (2001).

[59] C.-S. Shin, D. Gall, Y.-W. Kim, P. Desjardins, I. Petrov, J. E. Greene, M. Odén, and L. Hultman, J. Appl. Phys. **90**, 2879 (2001).

[60] W. N. Shafarman and T. G. Castner, Phys. Rev. B **33**, 3570 (1986).

[61] W. N. Shafarman, D. W. Koon, and T. G. Castner, Phys. Rev. B **40**, 1216 (1989).

[62] E. Abrahams, P. W. Anderson, D. C. Licciardello, and T. V. Ramakrishnan, Phys. Rev. Lett. **42**, 673 (1979).

[63] G.A. Thomas, Y. Ootuka, S. Katsumoto, S. Kobayashi, and W. Sasaki, Phys. Rev. B **25**, 4288 (1982).

[64] M. Hering, M. Scheffler, M. Dressel, and H. V. Löhneysen, Phys. Rev. B **75**, 205203 (2007).

[65] M. A. Paalanen, T. F. Rosenbaum, G. A. Thomas, and R. N. Bhatt, Phys. Rev. Lett., **51**, 1896 (1983).

[66] Charles Kittel, “Introduction to solid state physics,” 7th edition, Wiley, Hoboken, NJ, USA (1995).

[67] O. Madelung, "Introduction to Solid-State Theory", Springer Verlag, Berlin, (1978).

[68] D. Gall, I. Petrov, and J. E. Greene, J. Appl. Phys. **89**, 401 (2001).

[69] E. A. Davis, and W. D. Compton, Phys. Rev. A **140**, 2183 (1965).

[70] P. W. Anderson, Phys. Rev. **109**, 1492 (1958).

[71] L. Friedman, J. Non-Cryst. Solids **6**, 329 (1971).

[72] V. F. Gantmakher, “Electrons and disorder in solids”, Clarendon Press, Oxford, UK (2005).

[73] C. X. Quintela, F. Rivadulla, and J. Rivas, Phys. Rev. B **82**, 245201 (2010).

[74] A. M□bius, Solid. State. Commun. **73**, 215 (1990).

Figure captions

Figure 1: (a) XRD ω-2θ scan from a 1-µm-thick CrN/MgO(001) sample. The inset shows a corresponding ω-rocking curve for the CrN 002 reflection at $2\theta = 43.26°$. (b) Width Γ_ω of the CrN 002 rocking-curve peak and the in-plane XRD coherence length $\eta_{||}$ vs T_s.

Figure 2: (a) Conductivity σ at room temperature (290 K) and 10 K vs the growth temperature T_s = 550-850 °C of 140-nm-thick CrN/MgO(001) layers. (b) Semi-log plot of the CrN conductivity vs reciprocal temperature. The open symbols represent the measured data for samples grown at different T_s. The solid lines are the result from nonlinear curve fitting, using equations (9) and (10).

Figure 3: Conductivity σ of three CrN/MgO(001) layers grown at T_s = 550, 700 and 850 °C, plotted on a log-scale vs (a) $T^{1/4}$ and (b) $T^{1/2}$. The lines are obtained from linear fitting in the temperature ranges of 50-120 K and 10-25 K for (a) and (b), respectively.

Figure 4: Localization length ξ vs T_s. The right y-axis indicates the corresponding lower limit for the N-vacancy concentration N_v.

Figure 5: Log-log plot of the normalized conductivity vs normalized temperature for all samples. The solid line corresponds to the scaling function in Eq. (10).

Figure 6: Optical reflectance R vs wavelength from 140-nm-thick CrN/MgO(001) layers grown at T_s = 550-850 °C, measured with an incident angle of 45°.

Figure 1

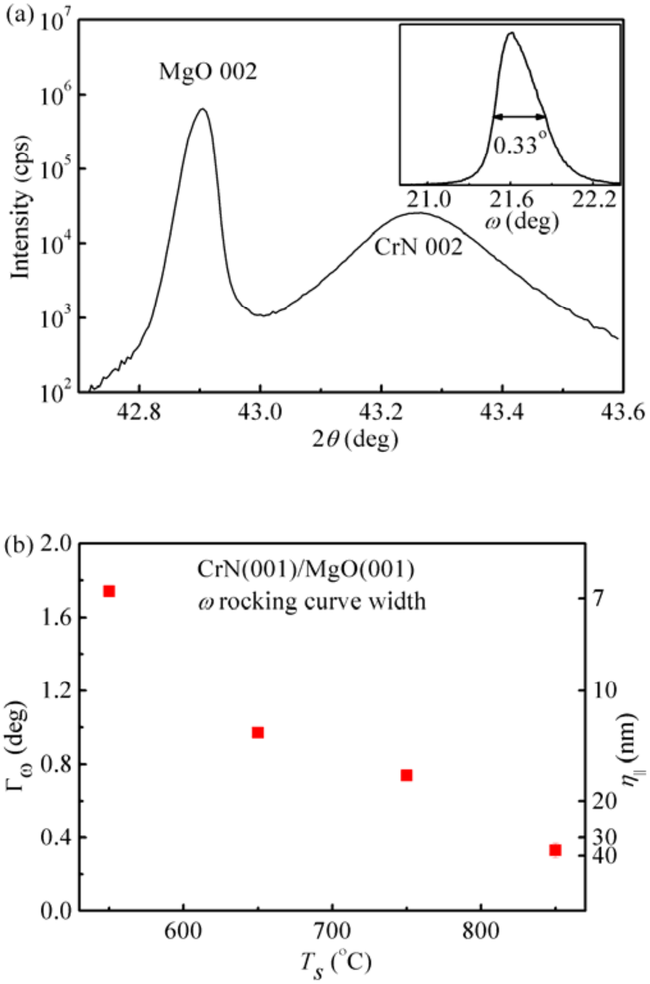
(a)
Intensity (cps)
10^7
10^6
10^5
10^4
10^3
10^2
MgO 002
CrN 002
42.8
43.0
43.2
43.4
43.6
2θ (deg)
0.33°
21.0
21.6
22.2
ω (deg)
(b)
2.0
1.6
1.2
0.8
0.4
0.0
Γ_ω (deg)
CrN(001)/MgO(001)
ω rocking curve width
7
10
20
30
40
$\eta_\parallel$ (nm)
600
700
800
T_s (°C)

Figure 2

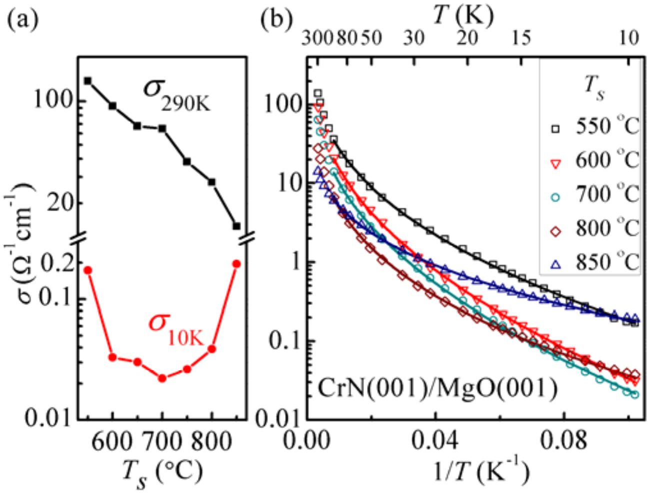
(a)
(b)
σ_{290K}
σ_{10K}
100
20
0.2
0.1
0.01
σ (Ω^{-1}cm^{-1})
600
700
800
T_s (°C)
T (K)
300
80
50
30
20
15
10
100
10
1
0.1
0.01
0.00
0.04
0.08
1/T (K^{-1})
T_s
550 °C
600 °C
700 °C
800 °C
850 °C
CrN(001)/MgO(001)

Figure 3

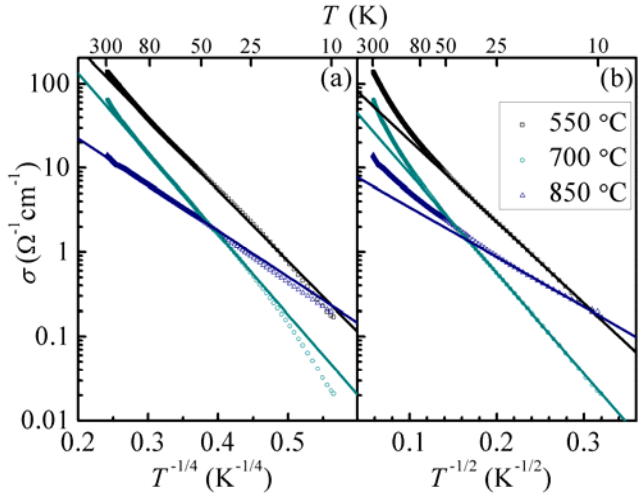
T (K)
300
80
50
25
10
300
80
50
25
10
(a)
(b)
550 °C
700 °C
850 °C
σ (Ω⁻¹cm⁻¹)
100
10
1
0.1
0.01
0.2
0.3
0.4
0.5
0.1
0.2
0.3
T^-1/4 (K^-1/4)
T^-1/2 (K^-1/2)

Figure 4

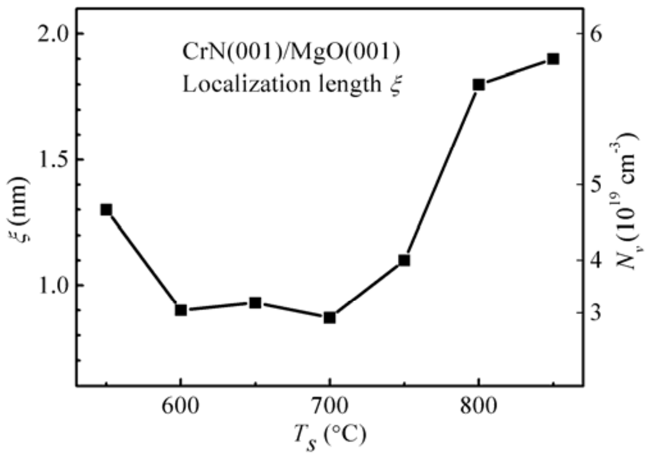
CrN(001)/MgO(001)
Localization length ξ
ξ (nm)
2.0
1.5
1.0
N_v (10^{19} cm^{-3})
6
5
4
3
600
700
800
T_S (°C)

Figure 5

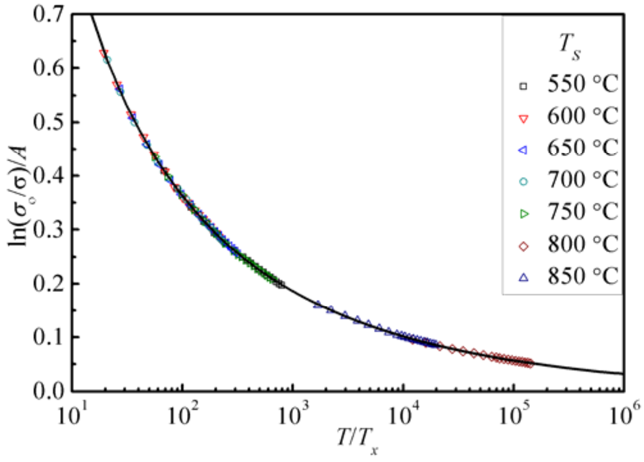
0.7
0.6
0.5
0.4
0.3
0.2
0.1
0.0
$\ln(\sigma_o/\sigma)/A$
10^1
10^2
10^3
10^4
10^5
10^6
T/T_x
T_S
550 °C
600 °C
650 °C
700 °C
750 °C
800 °C
850 °C

Figure 6

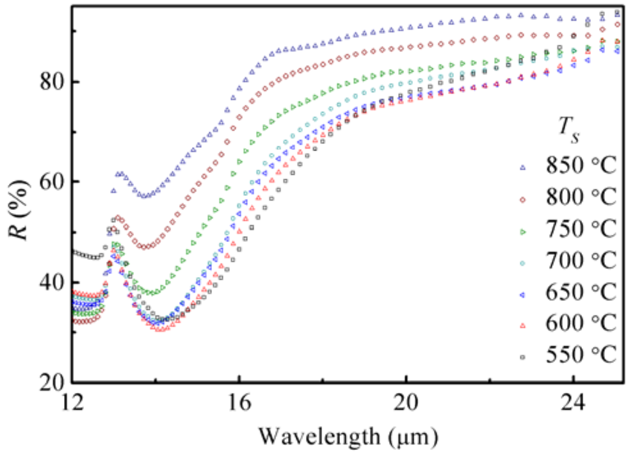
R (%)
20
40
60
80
12
16
20
24
Wavelength (μm)
T_S
850 °C
800 °C
750 °C
700 °C
650 °C
600 °C
550 °C

Table Captions

Table I: Parameters obtained from Mott and ES VRH fitting for T = 50-120 K and T = 10-25 K, respectively, from seven epitaxial CrN(001) layers grown at different T_s = 550-850 °C.

Table II: Parameters obtained by fitting CrN(001) conductivity data with universal scaling equations, i.e. Eqs. 9 and 10, over the temperature range T = 10-120K.

Table I

T_s (°C)	T_M (10^3 K)	T_{ES} (K)	ξ (nm)	Δ_{CG}/k (K)	T^* (K)
550	142	498	1.3	29.5	28.0
600	215	723	0.90	41.4	37.9
650	219	704	0.93	39.9	36.2
700	234	749	0.87	42.4	38.4
750	167	586	1.1	34.7	32.9
800	186	393	1.8	18.1	13.3
850	25.2	186	1.9	16.0	21.9

Table II

T_s (°C)	A (arb. u.)	lnσ_o (Ω^{-1}cm^{-1})	T_x (K)	T'_M (10^3 K)	T'_{ES} (K)
550	25.0	8.44	0.144	56	404
600	18.6	8.20	0.505	59.8	782
650	20.5	7.93	0.362	63.4	682
700	18.9	7.76	0.469	59.9	754
750	25.9	7.60	0.176	78.8	529
800	115	7.76	0.000804	142	48.1
850	45.9	5.70	0.00582	25.7	55.0